ACS APPLIED MATERIALS & INTERFACES

Research Article

www.acsami.org

Visible-Light-Responsive Photocatalysts toward Water Oxidation Based on NiTi-Layered Double Hydroxide/Reduced Graphene Oxide Composite Materials

Bei Li, Yufei Zhao, Shitong Zhang, Wa Gao, and Min Wei*

State Key Laboratory of Chemical Resource Engineering, Beijing University of Chemical Technology, Beijing 100029, P. R. China

Supporting Information

ABSTRACT: A visible-light responsive photocatalyst was fabricated by anchoring NiTi-layered double hydroxide (NiTi-LDH) nanosheets to the surface of reduced graphene oxide sheets (RGO) via an in situ growth method; the resulting NiTi-LDH/RGO composite displays excellent photocatalytic activity toward water splitting into oxygen with a rate of 1.968 mmol g^{-1} h^{-1} and a quantum efficiency as high as 61.2% at 500 nm, which is among the most effective visible-light photocatalysts. XRD patterns and SEM images indicate that the NiTi-LDH nanosheets (diameter: 100−200 nm) are highly dispersed on the surface of RGO. UV−vis absorption spectroscopy exhibits that the introduction of RGO enhances the visible-light absorption range of photocatalysts, which is further verified by the largely decreased band gap (~1.78 eV) studied by cyclic voltammetry measurements. Moreover, photoluminescence (PL) measurements indicate a more efficient separation of electron−hole pairs; electron spin resonance (ESR) and Raman scattering spectroscopy confirm the electrons transfer from NiTi-LDH nanosheets to RGO, accounting for the largely enhanced carrier mobility and the resulting photocatalytic activity in comparison with pristine NiTi-LDH material. Therefore, this work demonstrates a facile approach for the fabrication of visible-light responsive NiTi-LDH/RGO composite photocatalysts, which can be used as a promising candidate in solar energy conversion and environmental science.

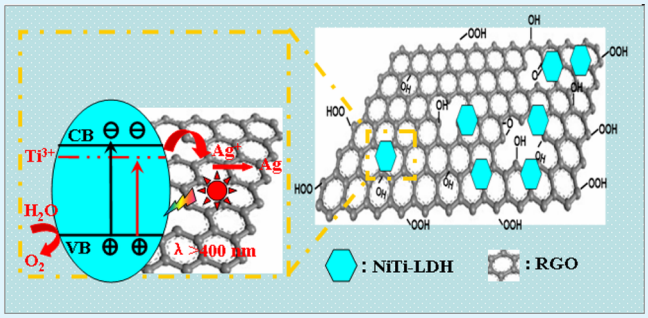

KEYWORDS: *visible-light response, photocatalysts, water oxidation, reduced graphene oxide, layered double hydroxides, composite materials*

1. INTRODUCTION

How to convert solar energy into clean fuels has received considerable attention for solving the global energy problem, and one of the most efficient approaches is to utilize the solar energy through photocatalysts to split water into H_2 and O_2 molecules.[1−4] TiO_2-based semiconductors are the most commonly used photocatalysts for water splitting, but they are only active upon UV excitation in the 3−5% of solar energy,[1] which limits their further applications. Many attempts have been explored to sensitize TiO_2 for the visible-light response by doping or hydrogenation route.[5] However, the visible optical absorption of these modified materials under sunlight is still unsatisfactory and thus results in low photoactivities. Therefore, novel and efficient visible-light-driven photocatalysts are extremely essential to meet the requirements of environment and solar energy conversion.

Layered double hydroxides (LDHs),[6−11] whose structure can be described by the formula $[M^{2+}_{1-x}M^{3+}_{x}(OH)_2]^{x+}(A^{n-})_{x/n}\cdot mH_2O$ (M^{2+} and M^{3+} are di- and trivalent metal cations of host layer; A^{n-} is n-valent interlayer exchangeable guest anions), are a large class of important layered anionic clays. Owing to the specific structure and versatility in chemical composition, they have been widely used as semiconductor materials in the fields of photocatalytic water splitting and degradation of environmental pollutants.[12−15] For instance, Silva and Bouizi et al. reported the visible light photocatalytic behavior of ZnCr-LDH, which is superior to that of WO_3.[8] Our group studied a family of photoresponsive MTi-LDHs (M = Ni, Zn, Mg) for water splitting into hydrogen.[12] However, in these cases, unfortunately, a poor carrier mobility is normally inevitable, which leads to serious recombination of electron−hole and the resulting low catalytic efficiency. As a result, several attempts have been explored to improve the electric conductivity of LDHs-based photocatalysts by incorporation of carbon materials[16−20] or conductive polymers.[21,22]

Reduced graphene oxide (RGO), composed of the atomically thin layer of sp^2 hybridized carbon atoms arranged in a honeycomb lattice with hydroxyl and epoxy groups on the basal planes, has been regarded as an outstanding support material for the giant carrier mobility and large specific surface area.[23−28]

Received: July 23, 2013
Accepted: September 25, 2013
Published: September 25, 2013

Chen and Ohta et al. discovered that RGO serves as the electron acceptor when covalently bonded to electron-donating compounds like tetrathiafulvalene (TTF), or becomes the electron donator when combined with electron-absorbing species such as tetracyanoethylene (TCNE).[29−31] Zhou et al. reported that NiO/graphene oxide composites facilitate fast electron hopping from graphene oxide to NiO, which allows a high reversible capacity and excellent rate performance in lithium storage.[16] This motivates us to take the challenge of fabricating composite photocatalysts by immobilizing NiTi-LDH nanosheets on the surface of RGO, which would exhibit the following advantages: first, the presence of RGO enhances the carrier mobility and improves the photogenerated electron−hole separation efficiency of NiTi-LDH nanosheets; second, the large specific surface area of RGO allows sufficient exposure of LDH active sites, which would result in superior photocatalytic performances.

In this work, visible-light-driven NiTi-LDH/RGO catalysts were fabricated by anchoring NiTi-LDH nanosheets onto the surface of RGO via an in situ growth method, which display excellent photocatalytic behavior in water splitting into oxygen. TEM images of NiTi-LDH/RGO show that the NiTi-LDH nanosheets (diameter: 100−200 nm) are highly dispersed on the surface of RGO sheets; photoluminescence (PL) measurements indicate a more efficient separation of electron−hole pairs for the obtained NiTi-LDH/RGO composites compared with the pristine NiTi-LDH. The material of NiTi-LDH/2% RGO exhibits a maximum oxygen generation rate of 1.968 mmol g^{-1} h^{-1} and a brilliant apparent quantum efficiency of 61.2% at 500 nm, which is among the most effective visible-light photocatalysts. Electron spin resonance (ESR) and Raman scattering indicate the electron transfer from NiTi-LDH nanosheets to RGO, resulting in the largely enhanced carrier mobility and photocatalytic activity. Moreover, UV−vis absorption measurements reveal a broad absorption in visible-light region for the NiTi-LDH/RGO composite, which is further verified by a decreased band gap (∼1.78 eV) studied by cyclic voltammetry measurements.

2. EXPERIMENTAL SECTION

2.1. Material. $TiCl_4$ and crystalline flake graphite were purchased from Sigma-Aldrich Co. Chemical reagents including $KMnO_4$, $Ni(NO_3)_2{\cdot}6H_2O$, $Zn(NO_3)_2{\cdot}6H_2O$, $Cr(NO_3)_3{\cdot}9H_2O$, Na_2CO_3, NaOH, $NaNO_3$, urea, concentrated hydrochloric acid, concentrated sulphuric acid, H_2O_2 (30%) and ethanol were obtained from Beijing Chemical Co. Deionized water was used in the whole experimental process.

2.2. Synthesis of NiTi-LDH/RGO. Graphene oxide (GO)[32−35] was synthesized from crystalline flake graphite by a modified Hummers' method.[32] Subsequently, thermodynamically stable carbon oxide species (confirmed by Dreyer et al)[33] were produced from GO through a thermal exfoliation in order to get the reduced graphene oxide (RGO) (see details in the Supporting Information and Figure S1−S3). The synthesis of NiTi-LDH/RGO was similar to the coprecipitation method reported by our group previously.[14]

Preparation of NiTi-LDH/2.0%RGO with Various Ni^{2+}/Ti^{4+} Atomic Ratios. Four NiTi-LDH/2.0%RGO photocatalysts with various Ni/Ti molar ratios (Ni/Ti = 2, 3, 4, 5) were prepared by using an *in situ* growth method. The monolayer RGO suspension (2.0 wt % of the NiTi-LDH catalyst) was obtained by sonication (150 W, 40 min) in the 100 mL deionized water.[36] $Ni(NO_3)_2{\cdot}6H_2O$, $TiCl_4$ solution and 0.1 mol urea with various Ni:Ti molar ratios were dissolved in the above RGO suspension (the $TiCl_4$ solution: 0.5 mL; the solution was prepared with a volume ratio of 1:1 from 0.002 mol $TiCl_4$ to concentrated hydrochloric acid). After the solution was stirred vigorously (24 h) at a refluxing temperature (90 °C), the final precipitate was collected by centrifugation and rinsed thoroughly with an ethanol solution (1:1, v/v). The obtained product was dried in an oven at 60 °C for 24 h.

Preparation of NiTi-LDH/xRGO with Various RGO Content. Seven NiTi-LDH/*x*RGO photocatalysts (x = 0, 0.5, 1.0, 1.5, 2.0, 2.5, and 3.0 wt %) were prepared by using the same in situ growth method. The monolayer RGO suspension (with different weight percentage) was obtained by sonication (150 W, 40 min) in the 100 mL deionized water.[36] $Ni(NO_3)_2{\cdot}6H_2O$, $TiCl_4$ solution, and 0.1 mol urea (Ni/Ti = 4/1) were dissolved in the above RGO suspension. The following synthetic process is the same as described above.

For comparison, the sample of ZnCr-LDH, which has been reported as one of the most effective visible-light photocatalysts for O_2 production, was synthesized by the method introduced by Silva et al.[8]

2.3. Photocatalytic Tests. The photocatalytic experiments were conducted in a 50 mL Pyrex flask containing NiTi-LDH/RGO (50 mg) aqueous suspension (45 mL), with $AgNO_3$ (0.5 mmol) as a sacrificial reagent. The head space of reactor was sealed with an airtight silicon stopper, and the photocatalyst suspensions were purged thoroughly with argon for 30 min. A xenon arc lamp (300 W; Beijing AuLight Co., Ltd.) was used as a light source. Light was passed through a UV cutoff filter (λ > 400 nm) and then focused on the reactor. The reactor was kept at 40 °C in the water bath equipment in order to avoid the ambient temperature variation influence. The formation of oxygen was identified by injecting the reactor headspace gas in a gas chromatograph (GC-7890II; Techcomp. Co., Ltd.) operated under the isothermal conditions (30 °C) equipped with a semicapillary column and a thermal conductivity detector. The apparent quantum efficiency (AQE) was measured by utilizing potassium ferrioxalate as chemical actinometer.[8,37−39]

2.4. Material Characterization. Powder X-ray diffraction (XRD) patterns of the samples were recorded by a Shimadzu XRD-6000 diffractometer using Cu Kα radiation in a scan step of 0.02° and a scan range between 5° and 70°. Content analysis of metals was performed by ICP atomic emission spectroscopy on a Shimadzu ICPS-7500 instrument using the solutions prepared by dissolving the samples in dilute hydrochloric acid. UV−vis diffuse reflectance spectra of solid samples were recorded with a Beijing PGENERAL TU-1901 spectrometer in the 200−800 nm wavelength range. Fourier transform infrared spectra (FTIR) were collected using a Vector22 (Bruker) spectrophotometer with 2 cm^{-1} resolution in the range between 4000 and 400 cm^{-1}. The morphology of the samples was investigated using a scanning electron microscope (SEM, Zeiss Supra 55 with an accelerating voltage of 20 kV) which combines with energy-dispersive X-ray spectroscopy (EDX) performed in an Oxford Instruments INCA analyzer for determination of metal composition. A transmission electron microscopy (TEM, Philips Tecnai 20 with operated at 200 kV) and a high-resolution transmission electron microscope (HRTEM, JEOL JEM-2010 with an accelerating voltage of 200 kV) were used to study the structure of NiTi-LDH/RGO composite. Atomic force microscopy (AFM) images were collected using a Nano Scope IIIa AFM from Veeco Instruments in the tapping-mode in air. The specific surface area determination and pore volume were performed by Brunauer−Emmett−Teller (BET) and Barrett−Joyner−Halenda (BJH) methods, respectively, by use of a Quantachrome Autosorb-IC-VP analyzer. Analyzer X-ray photoelectron spectra (XPS) were recorded using a PHIQ2000 X-ray photoelectron spectrometer equipped with a monochromatized Al Kα X-ray source. Raman measurements were carried out using a Raman spectrometer (LabRAM ARAMIS) at 633 nm. The technique of the electron spin resonance (ESR) in N_2 atmosphere was applied to confirm the presence of active radicals formed on the pristine NiTi-LDH and NiTi-LDH/RGO materials. Fluorescence emission spectra were recorded using a fluorophotometer (RF-5301PC, 1.5 nm resolution) in the range 400−600 nm with the excitation wavelength of 350 nm and slit widths of 3 nm. An electrochemical workstation (CHI 660B, Shanghai Chenhua Instrument Co., China) was utilized for the cyclic voltammetry electrochemical measurements. A conventional three-electrode cell was used with a saturated Ag/AgCl electrode as the

reference, a platinum wire as the counter, and the NiTi-LDH/RGO modified glassy carbon electrode as the working electrode. The cyclic voltammetry curves were recorded in deaerated acetonitrile with $LiClO_4$ (0.01 mol/L) as the electrolyte at a scan rate of 0.1 V/s. All the measurements were performed at room temperature.

3. RESULTS AND DISCUSSION

3.1. Structure and Morphology of the NiTi-LDH/RGO Composite Materials. The NiTi-LDH/RGO composite materials were prepared successfully via an in situ growth method, whose XRD patterns are shown in Figure 1 and Figure S4 in the Supporting Information. It is found that the NiTi-LDH/RGO composites with various weight percentages of RGO exhibit rather similar XRD patterns. The peaks at 12, 24, 33, 37, and 60° 2θ can be indexed to the (003), (006), (009), (012), and (110) reflection of NiTi-LDH phase with *R*3*m* rhombohedral symmetry, respectively.[14,40] No typical diffraction peak of RGO is observed in these NiTi-LDH/RGO composites, which can be attributed to the superimposed characteristic reflection of RGO[41] at 24° 2θ (see Figure S1 in the Supporting Information), or to the rather low loading of RGO, which is below the detection limit of XRD. The elemental analysis results based on ICP-AES for these NiTi-LDH/RGO samples (see Table S1 in the Supporting Information) show that they possess close Ni/Ti molar ratio to the nominal one. Furthermore, FT-IR spectra (see Figure S5 in the Supporting Information) give the chemical composition and the LDH−RGO interaction information. Bands at 2229.6, 638, and 1383 cm^{-1} indicate the presence of cyanate anion (CNO^-), metal−NCO complex, and carbonate (CO_3^{2-}), respectively. The skeletal vibration of RGO[42] shows a red-shift from 1580 cm^{-1} (RGO, see Figure S5a in the Supporting Information) to 1623 cm^{-1} (NiTi-LDH/2%RGO, see Figure S5c in the Supporting Information), indicating that electron density in the benzenoid structure of RGO increases after combination with NiTi-LDH. In addition, the stretching vibration of C−OH in RGO moves from 3419 to 3427 cm^{-1} in the NiTi-LDH/2%RGO sample, suggesting the formation of hydrogen bonding between RGO and NiTi-LDH nanosheets.[43−45]

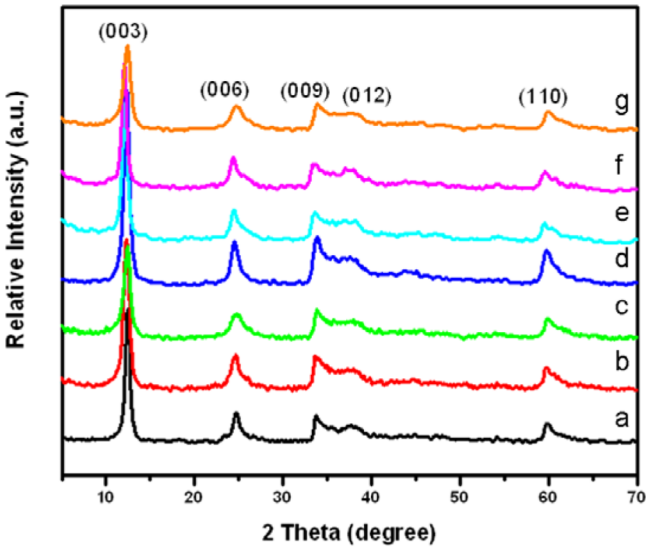

Figure 1. XRD patterns of the NiTi-LDH/*x*RGO composite materials. From a to g: x = 0, 0.5, 1.0, 1.5, 2.0, 2.5, and 3.0%, respectively. The molar ratio of Ni/Ti is 4/1.

Figure 2 shows SEM and TEM images of these samples. Different from the pristine NiTi-LDH material with serious aggregation (Figure $2A_1$), NiTi-LDH nanosheets on the surface of RGO carrier (Figure $2A_2$) are highly dispersed and have a platelike morphology with a lateral diameter of 100−200 nm (Figure 2B, B_1, and C). The elemental mapping images (Figure $2B_2$, B_3) display the uniform and homogeneous distribution of both Ni and Ti. In addition, the characteristic wrinkles of RGO on the edge (labeled by white dotted line) can be noticed from the TEM and HRTEM image of NiTi-LDH/2%RGO (Figure 2C, D). The lattice fringes in Figure $2D_1$ show the interplanar spacing of 0.36 nm, corresponding to the (006) lattice plane of NiTi-LDH phase. The BET surface area and pore size distribution of NiTi-LDH/RGO samples were investigated through adsorption−desorption measurements at 77 K (see Figure S6 in the Supporting Information). The introduction of RGO makes a significant enhancement in the specific surface area of composite material, i.e., from 123.83 m^2 g^{-1} (NiTi-

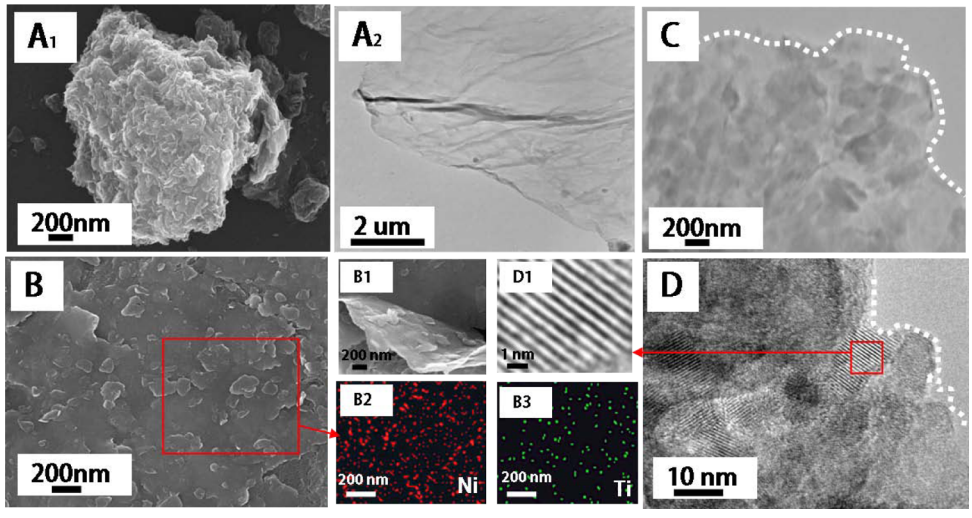

Figure 2. SEM images of (A_1) pristine NiTi-LDH, (B, B_1) NiTi-LDH/2%RGO with the elemental mapping images of (B_2) Ni and (B_3) Ti. (A_2) TEM image of RGO. (C) TEM and (D) HRTEM image of NiTi-LDH/2%RGO, with lattice fringe of NiTi-LDH shown in D_1.

LDH) to 224.61 m^2 g^{-1} (NiTi-LDH/2%RGO). The adsorption−desorption isotherm of NiTi-LDH/RGO composites are type IV with H3-type hysteresis loop (P/P_0 > 0.4), which indicates the predominant presence of mesopores.

Figure 3 displays UV−vis diffusion reflectance spectra of various NiTi-LDH/*x*RGO composites. The absorption spectrum of pure NiTi-LDH material presents two strong absorption bands in the region 200−400 nm and 600−800 nm, which can be attributed to the ligand-to-metal charge transfer and the existence of Ni cations in the host layer, respectively.[14] With the increase of the RGO content, the absorbance of the NiTi-LDH/*x*RGO composites in visible-light region enhances markedly. In addition, cyclic voltammetry measurements of these samples were performed to determine the energy gap which is obtained from the difference between oxidation and reduction potential.[46,47] As shown in Figure S7 in the Supporting Information, the energy gap decreases from NiTi-LDH (∼2.14 eV) to NiTi-LDH/2%RGO (∼1.78 eV). This result is consistent with the UV−vis diffuse reflectance spectra that the incorporation of RGO expands the absorption of NiTi-LDH to visible-light region, which imposes a key influence on the photocatalytic behavior of NiTi-LDH/RGO materials and will be discussed in the following section.

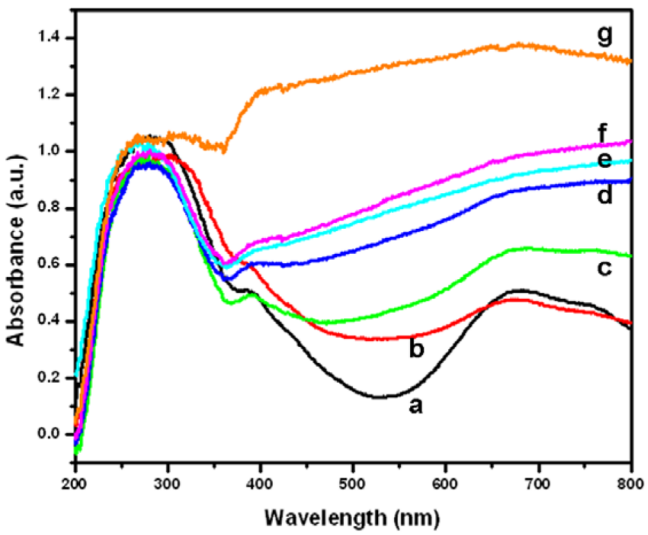

Figure 3. UV−vis diffusion reflectance spectra of various NiTi-LDH/*x*RGO composites. From a to g: *x* = 0, 0.5, 1.0, 1.5, 2.0, 2.5, and 3.0%, respectively.

3.2. Photocatalytic Activity Evaluation for NiTi-LDH/RGO Composite Materials. In this work, photocatalytic O_2 production results of NiTi-LDH/RGO samples were evaluated under visible-light irradiation, by using $AgNO_3$ as the sacrificial reagent which interacts with photogenerated electrons and leaves holes for water oxidation. Generally, the Ag 4d in Ag^+ can form new valence band in the photocatalyst system, which benefits the rapid separation of electron−hole pairs.[48] The influence of Ni/Ti molar ratio on the resulting photocatalytic behavior of NiTi-LDH/RGO was first studied (see Figure S8 in the Supporting Information), and the results show that the sample with Ni/Ti = 4/1 exhibits the optimal photocatalytic activity. As a result, this ratio was chosen for further investigation. The material of ZnCr-LDH, which has been reported as one of the most efficient photocatalysts toward water oxidation,[8] was used as a reference sample. It can be seen from Figure 4 that the pristine RGO shows no obvious photocatalytic activity toward water splitting; the NiTi-LDH material exhibits a low photocatalytic activity of 0.359 mmol g^{-1} h^{-1} O_2 generation rate under visible-light irradiation. However, the combination of RGO and NiTi-LDH leads to a significantly enhanced photocatalytic behavior. The oxygen productivity increases gradually from 1.228 mmol g^{-1} h^{-1} (NiTi-LDH/0.5% RGO) to 1.968 mmol g^{-1} h^{-1} (NiTi-LDH/2.0%RGO) along with the increase of RGO loading from 0.5% to 2.0%; while decreases sharply with further increase of RGO from 2.0% to 3.0%. The highest activity presents in the sample of NiTi-LDH/2.0%RGO. The first increase of RGO content (from 0.5% to 2.0%) results in the significantly accelerated carrier mobility and more exposed active centers, accounting for the improved photocatalytic activity, but an excessive loading of black color RGO (from 2.0% to 3.0%) would depress the light intensity utilized by catalytic active centers.[49,50] In addition, the resulting metallic Ag derived from $AgNO_3$ sacrificial reagent was studied by HRTEM (see Figure S9 in the Supporting Information), and the results show that the produced Ag was deposited on the surface of NiTi-LDH/2.0%RGO as nanoparticles, which may not impose obvious influence on the light absorption. The stability and recyclability of the NiTi-LDH/2.0%RGO sample were also tested, and the results show a slight decrease in oxygen production rate (see Figure S10A in the Supporting Information) and the undamaged structure of NiTi-LDH/2.0%RGO (see Figure S10B in the Supporting Information) after ten cycles. The results demonstrate that the NiTi-LDH/2.0%RGO composite material can be used as a promising photocatalyst for water oxidation with high activity and repeatability.

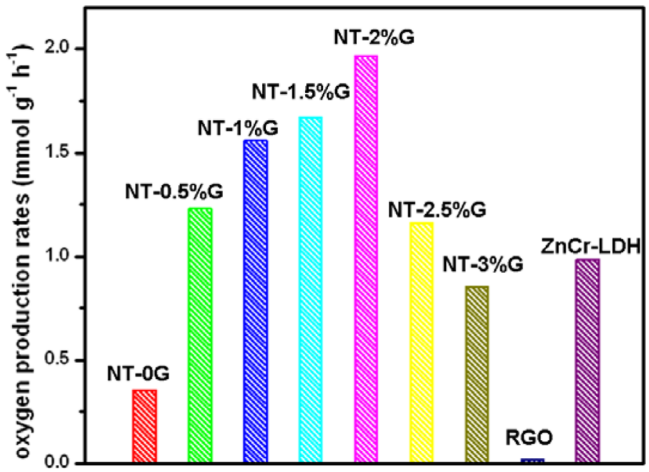

Figure 4. Comparison study on the photocatalytic O_2 production activity under visible-light irradiation over NiTi-LDH/*x*RGO composites denoted as NT-*x*G (*x* = 0, 0.5, 1.0, 1.5, 2.0, 2.5, 3.0%), with pristine RGO and ZnCr-LDH material as reference samples.

To give a further insight into the photocatalytic efficiency of NiTi-LDH/2%RGO, the corresponding apparent quantum efficiency (AQE) at various wavelengths was obtained by using potassium ferrioxalate as chemical actinometer. The measurements were carried out under the same photocatalytic reaction condition except the monochromatic filter was added to the xenon arc lamp for the monochromatic light source to trigger the water splitting. The varied quantum efficiencies at different visible absorption bands of NiTi-LDH/2%RGO are

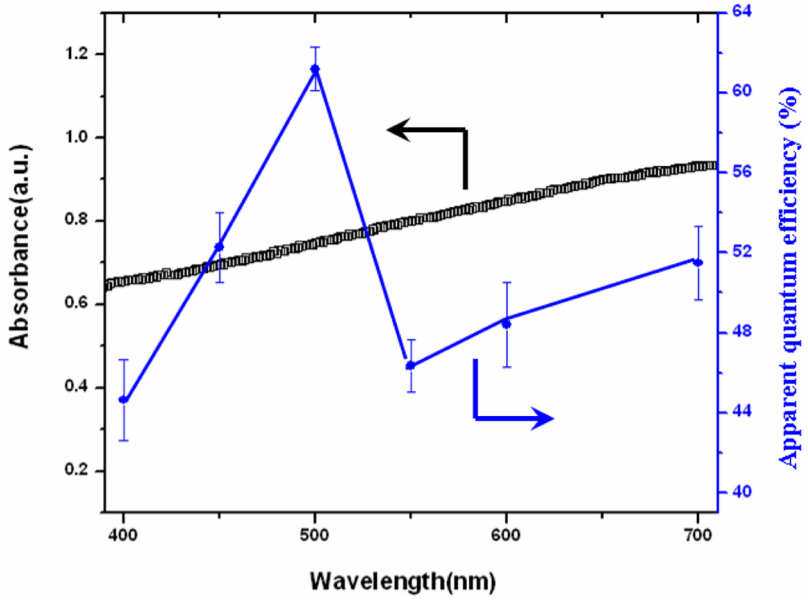

Figure 5. Diffuse reflectance UV−vis spectra (left vertical axis) of NiTi-LDH/2%RGO and apparent quantum efficency ($\Phi_{apparent}$) of incident photon to oxygen conversion (right vertical axis).

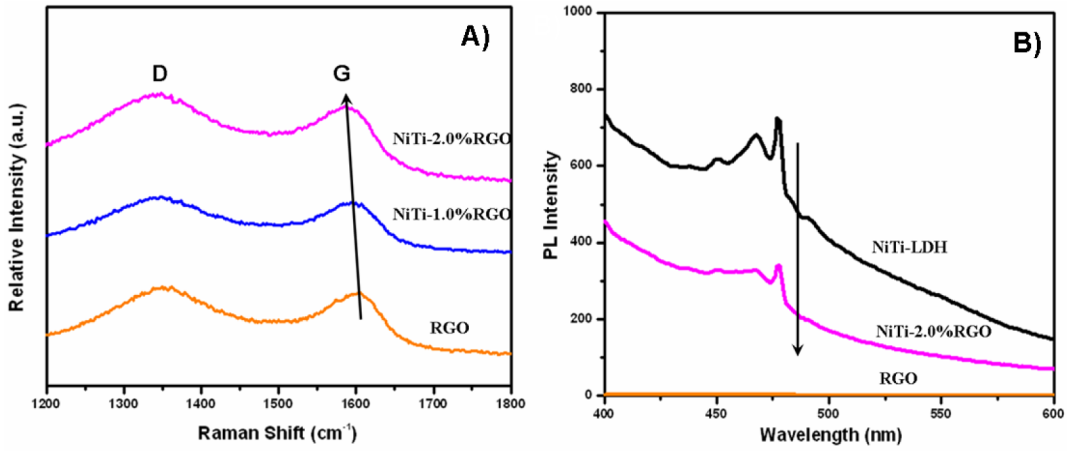

Figure 6. (A) G-band Shift in the Raman spectra of pristine RGO, NiTi-LDH/1.0%RGO and NiTi-LDH/2.0%RGO. (B) Photoluminescence spectra of RGO, NiTi-LDH, and NiTi-LDH/2%RGO, respectively.

due to the different nature of the electronic transition at each wavelength.[8] The AQE in Figure 5, especially at 500 nm (61.2%), is quite noteworthy, demonstrating NiTi-LDH/2% RGO as one of the most effective catalysts toward water splitting for O_2 generation upon visible-light irradiation.

3.3. Discussion on Structure−Property Correlation. *Photogenerated Electron−Hole Separation.* To get further insights into the largely enhanced photocatalytic activity of NiTi-LDH/RGO composites in comparison with pristine NiTi-LDH, we investigated Raman spectra on the NiTi-LDH/RGO materials by observing the shift of G-peak of RGO, which is due to bond stretching of sp^2 carbon pairs in both rings and chains.[24] As shown in Figure 6A, G-peak moves gradually from 1603 cm^{-1} (RGO) to 1586 cm^{-1} (NiTi-LDH/2%RGO), as a result of the LDH−RGO interaction. It has been reported that the G-peak shift in RGO is associated with doping effect. Specifically, when RGO interacts with electron donator, n-doping can be induced (G-peak shifts to low frequency); otherwise p-doping of RGO can be triggered (G-peak shifts to high frequency) as encountering electron acceptor.[29−31,51,52] The low-frequency shifting of G-peak in this work indicates that RGO in the NiTi-LDH/RGO composite shows the n-doping character, which could import electrons induced by visible-light from NiTi-LDH and therefore reduce the electron−hole recombination. The transfer of the photoinduced electrons and holes would cause variations in photoluminescence (PL) signal of material.[53] In this study, the PL emission spectra of the samples of RGO, NiTi-LDH, NiTi-LDH/2%RGO were examined in the 400−600 nm wavelength range (Figure 6B). The pristine RGO shows no PL behavior at all. The NiTi-LDH/2%RGO composite exhibits much weaker PL intensity compared with that of NiTi-LDH at approximately 466 nm (λ_{ex} = 350 nm), which confirms that a lower electron−hole recombination for the NiTi-LDH/2%RGO photocatalyst. Both the results of Raman and PL spectra demonstrate that *n*-type doping character of RGO occurs in the NiTi-LDH/RGO material along with depressed electron−hole recombination, accounting for the remarkable water oxidation activity under visible-light irradiation.

Narrowing of Band Gap. ESR technique was employed to investigate the presence of active radicals formed on the photocatalyst. Figure 7A, B show the ESR spectra of the fresh

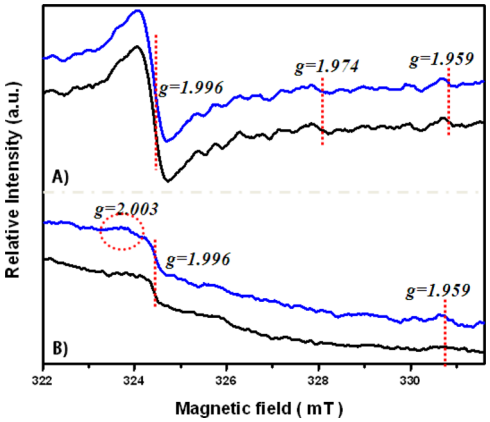

Figure 7. ESR spectra of (A) fresh NiTi-LDH/2%RGO before (black color) and after (blue color) visible-light irradiation for 30 min; (B) fresh NiTi-LDH before (black color) and after (blue color) visible-light irradiation for 30 min.

NiTi-LDH/2%RGO and NiTi-LDH as well as after visible-light irradiation for 30 min, respectively. The ESR signals of Ti^{3+} for the fresh NiTi-LDH/2%RGO (g = 1.996, g = 1.974, g = 1.959) in Figure 7A enhance greatly compared with those of fresh NiTi-LDH sample in Figure 7B, which are proportional to the content of Ti^{3+} in samples. It has been reported that Ti^{3+} species exhibits a specific visible light absorption, which can induce oxygen vacancy states between the conduction and valence band and thus improve the response toward visible light.[54−58] Therefore, the enhanced Ti^{3+} species in the sample of NiTi-LDH/2%RGO facilitates the decrease of its band gap, as verified by the cyclic voltammetry curves (see Figure S7 in the Supporting Information).

In addition, the sample of NiTi-LDH shows extra signal peaks of O_2^- (g = 2.003) and Ti^{3+} (g = 1.959) after irradiation (λ > 400 nm) in Figure 7B, which is possibly related to the acceptance the photogenerated electrons by Ti^{4+} and lattice oxygen.[59] However, similar result is not observed in the NiTi-LDH/2%RGO sample (Figure 7A), in which the peak intensities of Ti^{3+} remain almost unchanged and signal of O_2^- cannot be found after irradiation. The ESR results indicate the fast transfer of photogenerated electrons from NiTi-LDH to RGO upon irradiation, which is in agreement with the results of Raman spectra. In general, as shown in Figure 8, the presence of Ti^{3+} in the NiTi-LDH nanosheets facilitates the photogenerated electron−hole separation; whereas RGO with n-doping character transfers the electrons from NiTi-LDH to interact with $AgNO_3$ sacrificial agent and thus improves the oxidation efficiency of holes toward water splitting.

4. CONCLUSIONS

In summary, NiTi-LDH nanosheets grown on RGO have been achieved via an in situ growth method. The resulting NiTi-LDH/RGO composite materials display remarkable oxygen generation rate of water splitting upon visible-light irradiation. The sample of NiTi-LDH/2.0%RGO reaches a maximum O_2-production rate of 1.968 mmol g^{-1} h^{-1} with the AQE of 61.2% at 500 nm, about five times higher than that of bare NiTi-LDH and two times larger than that of ZnCr-LDH which is one of

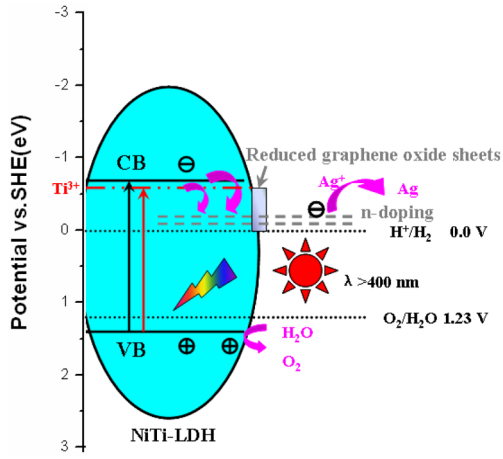

Figure 8. Schematic illustration of the charge separation and transfer in the NiTi-LDH/RGO system under visible-light irradiation.

the most efficient photocatalysts. Both Raman and PL spectra indicate that the *n*-doping character of RGO helps to transfer the photogenerated electrons from NiTi-LDH to interact with sacrificial agent Ag^+ and thus reduce the electron−hole recombination. In addition, the ESR spectra demonstrate that the abundant Ti^{3+} species in NiTi-LDH/RGO composite results in a stronger absorption in the visible-light range and enhances photocatalytic utilization rate of solar energy, in high accordance with the results of UV−vis diffusion reflectance spectra. Therefore, by virtue of the visible-light responsive photocatalysis of NiTi-LDH and the brilliant carrier mobility of RGO, the highly active photocatalyst demonstrated in this work can be potentially used in water splitting and solar energy conversion.

■ ASSOCIATED CONTENT

Supporting Information

The experimental details of preparation of RGO; the XRD patterns and O_2 evolution results of NiTi-LDH/2.0%RGO with different molar ratios of Ni/Ti; the elemental analysis of the NiTi-LDH/*x*RGO composite materials; FTIR spectra, nitrogen adsorption−desorption isotherms, and cyclic voltammetry curves of the NiTi-LDH/2%RGO (Ni/Ti = 4/1); XRD patterns, HRTEM, HADDF-STEM ,and elemental mapping images of the used NiTi-LDH/2%RGO (Ni/Ti = 4/1); the stability and recyclability of the NiTi-LDH/2.0%RGO (Ni/Ti = 4/1) catalyst. This material is available free of charge via the Internet at http://pubs.acs.org/.

■ AUTHOR INFORMATION

Corresponding Author

*E-mail: weimin@mail.buct.edu.cn. Phone: +86-10-64412131. Fax: +86-10-64425385.

Notes

The authors declare no competing financial interest.

■ ACKNOWLEDGMENTS

This work was supported by the 973 Program (Grant 2011CBA00504), the National Natural Science Foundation of China (NSFC), and the Beijing Natural Science Foundation (2132043). M.W. particularly appreciates the financial aid from the China National Funds for Distinguished Young Scientists of the NSFC.

REFERENCES

(1) Fujishima, A.; Honda, K. *Nature* **1972**, *238*, 37−38.
(2) Matsuoka, M.; Kitano, M.; Takeuchi, M.; Tsujimaru, K.; Anpo, M.; Thomas, J. M. *Catal. Today* **2007**, *122*, 51−61.
(3) Nowotny, J.; Sorrell, C. C.; Sheppard, L. R.; Bak, T. *Int. J. Hydrogen Energy* **2005**, *30*, 521−544.
(4) Kato, H.; Asakura, K.; Kudo, A. *J. Am. Chem. Soc.* **2003**, *125*, 3082−3089.
(5) Chen, X. B.; Liu, L.; Peter, Y. Y.; Samuel, S. M. *Science* **2011**, *331*, 746−750.
(6) Lin, Y.; Zhou, S.; Sheehan, W. S.; Wang, D. *J. Am. Chem. Soc.* **2011**, *133*, 2398−2401.
(7) Lee, Y. L.; Chi, C. F.; Liau, S. Y. *Chem. Mater.* **2010**, *22*, 922−927.
(8) Silva, C. G.; Bouizi, Y.; Fornes, V.; Garcia, H. *J. Am. Chem. Soc.* **2009**, *131*, 13833−13839.
(9) Williams, G. R.; O'Hare, D. *J. Mater. Chem.* **2006**, *16*, 3065−3074.
(10) Hu, G.; O'Hare, D. *J. Am. Chem. Soc.* **2005**, *127*, 17808−17813.
(11) Hetterley, R. D.; Mackey, R.; Jones, J. T. A.; Khimyak, Y. Z.; Fogg, A. M.; Kozhevnikov, I. V. *J. Catal.* **2008**, *258*, 250−255.
(12) Gong, M.; Li, Y. G.; Wang, H. L.; Liang, Y. Y.; Wu, J. Z.; Zhou, J. G.; Wang, J.; Regier, T.; Wei, F.; Dai, H. J. *J. Am. Chem. Soc.* **2013**, *135*, 8452−8455.
(13) Zhao, M. Q.; Zhang, Q.; Huang, J. Q.; Wei, F. *Adv. Funct. Mater.* **2012**, *22*, 675−695.
(14) Zhao, Y. F.; Chen, P. Y.; Zhang, B. S.; Su, D. S.; Zhang, S. T.; Tian, L.; Lu, J.; Li, Z. X.; Cao, X. Z.; Wang, B. Y.; Wei, M.; Evans, D. G.; Duan, X. *Chem.—Eur. J.* **2012**, *18*, 11949−11958.
(15) Zhao, Y. F.; Zhang, S. T.; Li, B.; Yan, H.; He, S.; Tian, L.; Shi, W. Y.; Ma, J.; Wei, M.; Evans, D. G.; Duan, X. *Chem.—Eur. J.* **2011**, *17*, 13175−13182.
(16) Zhou, G. M.; Wang, D. W.; Yin, L. C.; Li, N.; Li, F.; Cheng, H. M. *ACS. Nano* **2012**, *6*, 3214−3223.
(17) Zhu, P. N.; Nair, S.; Peng, S. J.; Yang, S. Y.; Ramarkrishna, S. *ACS Appl. Mater. Interfaces* **2012**, *4*, 581−585.
(18) Mu, J. B.; Shao, C. L.; Guo, Z. C.; Zhang, Z. Y.; Zhang, M. Y.; Zhang, P.; Chen, B.; Liu, Y. C. *ACS Appl. Mater. Interfaces* **2011**, *3*, 590−596.
(19) Tettey, K.; Yee, M. Q.; Lee, D. *ACS Appl. Mater. Interfaces* **2010**, *2*, 2646−2652.
(20) Zang, Y. Y.; Xie, D.; Wu, X.; Chen, Y.; Lin, Y. X. *Appl. Phys. Lett.* **2011**, *99*, 132904−132906.
(21) Han, J. B.; Dou, Y. B.; Zhao, J. W.; Wei, M.; Evans, D. G.; Duan, X. *Small* **2013**, *9*, 98−106.
(22) Mahanta, D.; Manna, U.; Madras, G.; Patil, S. *ACS Appl. Mater. Interfaces* **2011**, *3*, 84−92.
(23) Kong, B. S.; Geng, J. X.; Jung, H. T. *Chem. Commun.* **2009**, *16*, 2174−2176.
(24) Eda, G.; Chhowalla, M. *Adv. Mater.* **2010**, *22*, 2392−2415.
(25) Chen, C. M.; Zhang, Q.; Huang, C. H.; Zhao, X. C.; Zhang, B. S.; Kong, Q. Q.; Wang, M. Z.; Yang, Y. G.; Cai, R.; Su, D. S. *Chem. Commun.* **2012**, *48*, 7149−7151.
(26) Zeng, F. W.; Sun, Z. H.; Sang, X. G.; Diamond, D.; Lau, K. T.; Liu, X. X.; Su, D. S. *ChemSusChem* **2011**, *4*, 1587−1591.
(27) Rao, C. V.; Reddy, A. L. M.; Ishikawa, Y.; Ajayan, P. M. *ACS Appl. Mater. Interfaces* **2011**, *3*, 2966−2972.
(28) Mathkar, A.; Tozier, D.; Cox, P.; Ong, P. J.; Galande, C.; Balakrishnan, K.; Reddy, A. L. M.; Ajayan, P. M. *J. Phys. Chem. Lett.* **2012**, *3*, 986−991.
(29) Chen, W.; Chen, S.; Qi, D. C.; Gao, X. Y.; Wee, A. T. S. *J. Am. Chem. Soc.* **2007**, *129*, 10418−10422.
(30) Loh, K. P.; Bao, Q. L.; Ang, P. K.; Yang, J. X. *J. Mater. Chem.* **2010**, *20*, 2277−2289.
(31) Ohta, T.; Bostwick, A.; Seyller, T.; Horn, K.; Rotenberg, E. *Science* **2006**, *313*, 951−954.
(32) Cote, L. J.; Kim, F.; Huang, J. X. *J. Am. Chem. Soc.* **2009**, *131*, 1043−1049.
(33) Dreyer, D. R.; Park, S. J.; Bielawski, C. W.; Ruoff, R. S. *Chem. Soc. Rev.* **2010**, *39*, 228−240.
(34) Kim, J.; Cote, L. J.; Kim, F.; Yuan, W.; Shull, K. R.; Huang, J. X. *J. Am. Chem. Soc.* **2010**, *132*, 8180−8186.
(35) Kim, J.; Cote, L. J.; Huang, J. X. *Acc. Chem. Res.* **2012**, *45*, 1356−1364.
(36) Guo, P.; Song, H. H.; Chen, X. H. *J. Mater. Chem.* **2010**, *20*, 4867−4874.
(37) Braun, A. M.; Maurette, M. T.; Oliveros, E. *Photochemical Technology*; John Wiley & Sons: Chichester, U.K., 1991.
(38) Kuhn, H. J.; Braslavsky, S. E.; Schmidt, R. *Pure Appl. Chem.* **2004**, *76*, 2105−2146.
(39) Yan, H. J.; Yang, J. H.; Ma, G. J.; Wu, G. P.; Zong, X.; Lei, Z. B.; Shi, J. Y. *J. Catal.* **2009**, *26*, 165−168.
(40) Lee, Y.; Choi, J. H.; Jeon, H. J.; Choi, K. M.; Lee, J. W.; Kang, J. K. *Energy Environ. Sci.* **2011**, *4*, 914−920.
(41) Wu, Z. S.; Ren, W. C.; Wen, L.; Gao, L. B.; Zhao, J. P.; Chen, Z. P.; Zhou, G. M.; Li, F.; Cheng, H. M. *ACS Nano* **2010**, *4*, 3187−3194.
(42) Zhang, H.; Lv, X. J.; Li, Y. M.; Wang, Y.; Li, J. H. *ACS. Nano* **2010**, *4*, 380−386.
(43) Fan, J. J.; Liu, S. W.; Yu, J. G. *J. Mater. Chem.* **2012**, *22*, 17027−17036.
(44) Compton, O. C.; Nguyen, S. B. T. *Small* **2010**, *6*, 711−723.
(45) Guo, J. J.; Zhu, S. M.; Chen, Z. X.; Li, Y.; Yu, Z. Y.; Liu, Q. L.; Li, J. B.; Feng, C. L.; Zhang, D. *Ultrason. Sonochem.* **2011**, *18*, 1082−1090.
(46) Zhang, J. C.; Han, Z. Y.; Chen, M.; Yang, X. Y.; Cao, W. L. *J. Phys. Chem. Solids* **2010**, *71*, 1316−1323.
(47) Han, Z. Y.; Zhang, J. C.; Yang, X. Y.; Zhu, H.; Cao, W. L. *Org. Electron.* **2010**, *11*, 1449−1460.
(48) Kudo, A.; Miseki, Y. *Chem. Soc. Rev.* **2009**, *38*, 253−278.
(49) Zhang, Y. H.; Zhang, N.; Tang, Z. R.; Xu, Y. J. *ACS Nano* **2012**, *6*, 9777−9789.
(50) Zhang, J.; Yu, J. G.; Jaroniec, M.; Gong, J. R. *Nano Lett.* **2012**, *12*, 4584−4589.
(51) Jung, N. Y.; Kim, B. J.; Crowther, A. C.; Kim, N. D.; Nuckolls, C.; Brus, L. *ACS Nano* **2011**, *5*, 5708−5716.
(52) Das, B.; Voggu, R.; Rout, C. S.; Rao, C. N. R. *Chem. Commun.* **2008**, *41*, 5155−5157.
(53) Chakrapani, V.; Tvrdy, K.; Kamat, P. V. *J. Am. Chem. Soc.* **2010**, *132*, 1228−1229.
(54) Kormann, C.; Bahnemann, D. W.; Hoffmann, M. R. *J. Phys. Chem.* **1988**, *92*, 5196−5201.
(55) Bityurin, N.; Kuznetsov, A. I.; Kanaev, A. *Appl. Surf. Sci.* **2005**, *248*, 86−90.
(56) Xiong, L.; Ouyang, M.; Yan, L.; Qiu, M.; Yu, Y. *Chem. Lett.* **2009**, *38*, 1154−1155.
(57) Xiong, L. B.; Li, J. L.; Yang, B.; Yu, Y. *J. Nanomater.* **2012**, *2012*, 1−13.
(58) Hoang, S.; Berglund, S. P.; Hahn, N. T.; Bard, A. J.; Mullins, C. B. *J. Am. Chem. Soc.* **2012**, *134*, 3659−3662.
(59) Komaguchi, K. J.; Maruoka, T.; Nakano, H.; Imae, I.; Ooyama, Y.; Harima, Y. *J. Phys. Chem. C* **2010**, *114*, 1240−1245.